Development of IoT Slope Monitoring System and its Applications for Kratu-Patong Road Landslide in Phuket, Thailand

A. Jotisankasa[1], W. Praphatsorn[2], V. Siriyakorn[3], P. Sanposh[3], I. Janthong[2], Y. Tipsuwan[4], A. Sawangsuriya[5], and P. Jitareekul[6]

[1]*Department of Civil Engineering, Faculty of Engineering, Kasetsart University, Bangkok, Thailand*
[2]*Green Ground Solutions, Co. Ltd., Bangkok, Thailand*
[3]*Department of Electrical Engineering, Faculty of Engineering, Kasetsart University, Bangkok, Thailand*
[4]*Department of Computer Engineering, Faculty of Engineering, Kasetsart University, Bangkok, Thailand*
[5]*Bureau of Road Research and Development, Department of Highways, Thailand*
[6]*Bureau of Materials, Analysis and Inspection, Department of Highways, Thailand*
E-mail: fengatj@ku.ac.th

ABSTRACT: This paper presents an on-going development of Internet-of-Things (IoT) slope monitoring for landslide early warning system in Thailand. The current system employs a variety of sensors, namely MEMs-based tensiometers, piezometers, soil moisture sensor, tiltmeter, in-placed inclinometer and tipping bucket raingauge, all connected to Arduino-based microcontroller which relied on Narrowband, NB-IoT, protocol for data transmission to the cloud server. A specially designed application platform was developed to convert the sensor readings to engineering unit and ultimately geotechnical parameters, such as factor of safety, which enable engineers to readily understand the situation and make an informed-decision based on such parameters. A weighted approach was proposed in calculating the overall landslide hazard level based various kinds of sensor readings. A case history of Kratu-Patong Road Landslide in Phuket, Southern Thailand, taking place in Year 2022 was presented to demonstrate how the developed IoT system was used real-time together with geotechnical analysis to aid in traffic management during the critical time. The warning event primarily stemmed from spikes in slope movement, spurred by heightened traffic intensity. Rapid slope movement during the incident was characterized by a tilting magnitude of -2 to 1.2 degrees and a velocity ranging from -1.7 to 1.8 degrees per hour. Notably, the calculation of the warning index based on tilting magnitude provides a continuous warning message, in contrast to an intermittent message based on tilting velocity. The tensiometer effectively detected the decrease in suction caused by slope movement, while the piezometer only registered changes in pore-water pressure when the groundwater table rose above the measurement point. Finally, an Artificial Neural Network (ANN) model was used to predict the pore-water pressure at different depths based on 5 rainfall parameters, namely, 5-min, 1-hour, 1-day, 3-day and 7-day antecedent rainfalls. The model demonstrated satisfactory predictive accuracy (R^2 = 0.644, RMSE = 3.637 kPa), offering promising potential for integration with the IoT platform in the future.

KEYWORDS: IoT slope monitoring system, Slope stability, Landslide early warning, and Pore-water pressure.

1. INTRODUCTION

Instrumentation has been pivotal in the advancement of the geotechnical engineering profession from its beginning. By employing field observation and monitoring data, geotechnical engineers can effectively assess and make informed decisions regarding the design, construction, and maintenance of earth structures. Should the need arise, adjustments to the design can be implemented during the construction phase, under the condition that the gathered field information, supplemented by geotechnical analysis, substantiates such modifications. This approach is commonly referred to as the "learn as you go" method, coined by Karl Terzaghi, or the observational method, as proposed by Ralph Peck (Ridley, 2022).

The clarity of objectives is crucial when implementing geotechnical instrumentations. As noted by Ralph Peck in Dunnicliff and Green (1988), every instrument employed in a project should be carefully selected and strategically placed to address a specific question. Dunnicliff and Green (1988) identified multiple objectives of geotechnical instrumentation, which include: 1) safety (i.e. early warning system); 2) observational method; 3) construction control; 4) legal protection; 5) public relations; and 6) advancing the State-of-the-Art.

Ralph Peck, as highlighted in Ridley (2022), emphasizes the significance of promptly presenting field observations in a manner that effectively highlights the essential features, regardless of whether they are conducted in an elaborate and precise manner or quickly and informally. The true value of these observations lies in their usefulness, which is dependent on their timely display and clear representation. This approach ensures that the information remains up to date and readily accessible for decision-making purposes. The advent of Internet of Things (IoT) sensor technology enables monitoring of various parameters in-situ that can be accessed via web-based application in a real-time manner and thus makes this approach more economically feasible.

Rainfall-induced landslides have been increasingly prevalent and widespread worldwide, a trend attributable to climate change, extreme weather events, and rapid development in hilly areas. As a result, geotechnical engineers frequently encounter daunting challenges when these natural disasters occur, particularly when road networks are affected, leading to road blockages. The situation becomes even more complex as rectification efforts become necessary precisely when road users rely on the traffic lanes for their transportation needs. The convergence of these circumstances places geotechnical engineers in a critical position, requiring them to find the delicate balance between ensuring the safety and stability of the affected slopes and minimizing disruptions to the transportation network. In such situation, a slope monitoring system is needed which can provide real-time monitoring results, interpreted in such a manner that engineers can readily grasp the essence of the slope behaviour and use them for well-informed decision making.

In this study, an Internet of Things (IoT) slope monitoring system was presented consisting of a variety of sensors, namely MEMs-based tensiometers, piezometers, soil moisture sensor, tiltmeter, in-placed inclinometer and tipping bucket raingauge, all connected to Arduino-based microcontroller which relied on Narrowband, NB-IoT, protocol for data transmission to the cloud server. A specially designed application platform was developed to convert the sensor readings to engineering unit, geotechnical parameters, and a landslide hazard index that aid in decision making. A case history of Kratu-Patong Road Landslide in Phuket, Southern Thailand, in Year 2022 was then presented to demonstrate how the system was used to aid in traffic management.

2. IOT SLOPE MONITORING SYSTEM

2.1 Sensors

The developed IoT slope monitoring system consists of a variety of sensors schematically shown in Figure 1 (Jotisankasa et al., 2023). The sensors include MEMs-based tensiometers/piezometers, (Jotisankasa et al., 2015), soil moisture sensor, tiltmeter, in-placed inclinometer (Jotisankasa et al., 2023) and tipping bucket raingauge (Figure 2), all connected to Arduino-based microcontroller which relied on Narrowband, NB-IoT, protocol for data transmission to the cloud server. Both piezometer and tensiometer are based MEMs pressure sensor technology, incorporated with low-air entry filter for piezometer and high-air entry ceramic for tensiometer. The tensiometer's water reservior are carefully filled with deaired water as explained by Jotisankasa et al. (2015) and capable of measuring pore-water pressure in the range of -80 kPa to 700 kPa. While the tensiometers can measure negative pore-water pressure (i.e. suction) in slope, the piezometer can measure only positive pore-water pressure and should only be installed at the depth below the groundwater table.

The tiltmeter and in-place inclinometer utilize analog accelerometers with a sensitivity of 140 mV/deg and a maximum reading range of ±15 degrees. While both instruments serve their purpose, there are important distinctions between them. The tiltmeter is comparatively easier to install, but its functionality is limited to indicating slope surface movement only. The in-place inclinometer can measure the slope movement at varying depths and be used to estimate the lateral movement and thus determined the slip surface location. Though giving more information on slope behaviour, the in-place inclinometer requires specifically built borehole and is much more expensive to install than the tiltmeter. For shallow slide application, the tiltmeter, which is attached to a steel pole down to about 1m depth, tend to be much more cost-effective and easier to install. The primary advantage of both in-place inclinometer and tiltmeter in this study lies in its ability to monitor continuous movement in real-time, eliminating the need for frequent site visits to take measurements, as is the case with conventional inclinometer probes. This feature significantly reduces the hassle associated with data collection and analysis.

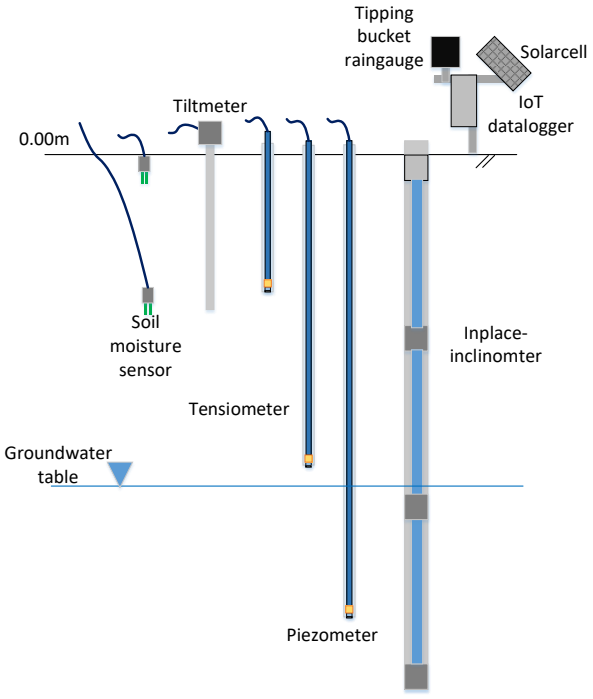

Figure 1 Schematic of the IoT sensors

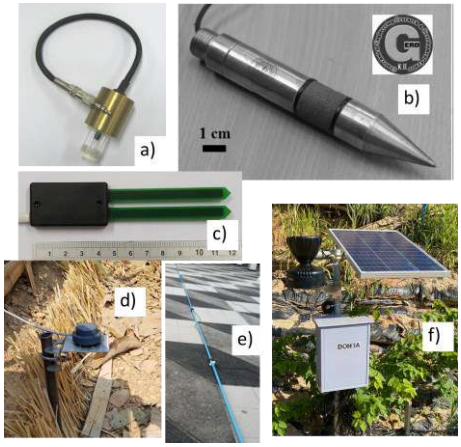

Figure 2 Photographs of the sensors; a) tensiometer, b) piezometer, c) soil moisture sensor, d) tiltmeter, e) in-place inclinometer and f) raingauge and IoT datalogger station

2.1 On-Line Slope Monitoring Platform

A web-based application was developed on a cloud server in order to process the data transmitted via the NBIoT network, specifically for slope engineering purposes. The core application is called Geotechnical Innovation Laboratory (GIL) platform. The transmitted sensor reading in raw unit, e.g. voltage, counts, etc, can then be converted to the engineering unit of interests (i.e. kPa, mm, degree, etc), by a user-specified conversion linear equation as follows;

$$\mathbf{Y} = (\mathbf{V} - \mathbf{V_i})/\mathbf{s} \quad (1)$$

where $\mathbf{V}$ is the sensor reading in raw unit, $\mathbf{Y}$ is the sensor reading in engineering unit, $\mathbf{V_i}$ is the initial zero the sensor reading (i.e. the reading in raw unit corresponding to the zero value in engineering unit, if $\mathbf{Y = 0}$, $\mathbf{V = V_i}$), and $\mathbf{s}$ is the sensor sensitivity. Typical values of sensitivity and initial zero for different sensors are summarized in Table 1. Notably, since the tensiometer and piezometer are based on absolute pressure sensor, their initial zero readings are dependent on the atmospheric pressure and thus on the elevation of the ground at the point of installation. The soil moistures sensor's calibration coefficients are also dependent on soil type and thus a separate calibration should be performed on the soil collected from the specific site where the sensor is installed as also highlighted by Jotisankasa et al. (2023). The GIL platform allows the users to specify all the calibration coefficients and thus capable of displaying the sensor's reading in engineering units in a real-time manner.

Accuracy and reliability of these sensors may be affected in long term deployment, particularly in adverse environmental conditions. Erratic readings, such as significant fluctuations in measurements, are indicative of sensor malfunction. It is advisable to conduct periodic checks on the sensors' zero readings and sensitivities annually. However, this process typically requires sensor removal and reinstallation, which can be resource-intensive in terms of both budget and time. These checks can be performed on-site for devices like the tensiometer and piezometer. One method involves filling the casing pipe with water to establish a known pressure head against which the sensor's reading can be compared.

Table 1 Typical calibration coefficients for different sensors

Sensor type	Sensitivity, s	Initial zero reading, V_i
Tensiometer/Piezometer	6.6 mV/kPa	780 to 850 mV
Tiltmeter/Inclinometer	-140 mV/Degree	2200-2600 mV
Soil moisture sensor	-105 mV/%	~4700 mV
Raingauge	1	0

2.1.1 Factor of Safety

For slope stability application, the factor of safety represents the main index that engineers readily understand as a measure of safety and stability of the slope. It is well known (e.g. Buscarnera, & di Prisco, 2011, Cascini et al., 2010, Jotisankasa et al., 2015) that for rainfall-induced landslide, it is the pore-water pressure that controls the effective stress, shear strength and ultimately the slope stability. The developed platform was thus designed so that the factor of safety can be processed and displayed in a real-time manner, based on the pore-water pressure measurement. As a first step, the infinite slope model was used to calculate the factor of safety, F, as shown in Equation (2) below.

$$F = \frac{c' + c_r + \gamma z \cdot \cos^2\beta \tan\phi' - u_w \tan\phi''}{\gamma z \sin\beta \cos\beta} \quad (2)$$

where γ is the total unit weight of soil, z is the depth of failure plane, β is slope angle, c' is effective cohesion intercept, c_r is root cohesion which is related to plant root reinforcement and root area ratio (e.g. Mahannopkul and Jotisankasa, 2019). The root cohesion can be assumed either as constant or as functions of depth. ϕ' is effective angle of shearing resistance, u_w is pore water pressure, and ϕ'' is the angle of shearing resistance due to pore-water pressure (positive or negative). For the case that u_w>0 (saturated soil), ϕ''equals ϕ'. For unsaturated soils, u_w<0 and ϕ''equals $\phi^b \sim tan^{-1}(S_r tan\phi')$. These parameters can be defined by users in the platform. It is however important to note that the infinite slope mode is used only as an initial estimate of the factor of safety. In reality, the slip surface may be slip circle or of irregular shape and the detailed slope stability analysis should be conducted to find the variations of F with pore-water pressure and used as input in the platform.

2.1.2 Critical Pore Water Pressure and Soil Moisture

It is noted that the threshold value of pore-water pressure at different values of factor of safety, F, can be calculated by rearranging the Equation (2) as follows.

$$u_{w,cr} = \frac{c' + c_r + \gamma z \cdot \cos^2\beta \tan\phi' - F \times \gamma z \sin\beta \cos\beta}{\tan\phi''} \quad (3)$$

This critical values of pore-water pressure at failure, $u_{w,cr}$, can then be estimated by setting the factor of safety equal to 1 as shown in Equation (3). Additional margin of safety can be added by inserting different values of F. Once the critical values of u_w is determined, the corresponding soil moisture at critical condition can then be estimated using the relevant soil-water retention curve (e.g. Kankanamge et al., 2018). It is interesting to note that an increase in root cohesion, c_r , due to slope vegetation can cause the critical pore-water pressure to rise, thus increasing the threshold for landslide warning. The effect of land cover on the landslide warning threshold can be specified in this manner.

2.1.3 Critical Rainfall Envelope

The rain pattern, plotted as daily rainfall versus antecedent rainfall (accumulated rain in previous few days), can provide a useful tool for roughly estimating when slope failure is likely to occur, as suggested by many previous researchers (e.g., Lumb, 1975, Crozier & Eyles, 1980, Mairaing et al., 2012). An example of such plot for a case history of Kratu-Patong road landslide in phuket, presented thereafter, is shown in Figure 3. The failure critical rainfall envelope demarcates the rainfall patterns that induced major landslide from the others that do not. The warning rainfall envelope sets the boundary of rain pattern that induce minor landslide.

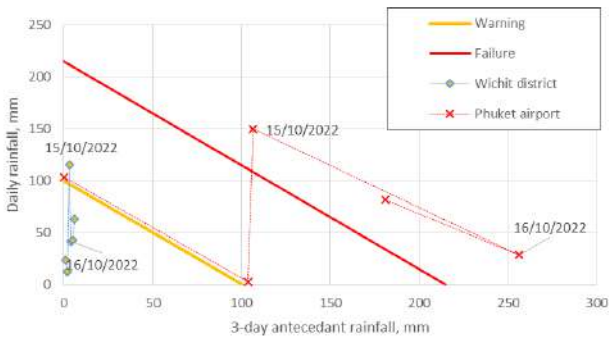

Figure 3 Critical rainfall envelope for Kratu-Patong road 2022 landslide in Phuket

2.1.4 Critical Slope Movement

Soil movement is commonly used as an index for indicating slope instability (e.g. Sheikh et al., 2021, Soralump et al., 2021, Jotisankasa et al., 2023). Tiltmeter attached to a rod driven onto slope surface (down to about 0.7 to 1 m deep) can be used to monitor the shallow slope movement, while inclinometer is traditionally used for detecting horizontal slope movement at greater depths. Either the movement magnitude (degree or mm) or movement rate (deg/h or mm/h) can be used to classify severity of movement. Based on Sheikh et al. (2021) the movement type is classified as very slow (<0.004 degree/h), slow (0.004-0.04 degree/h), moderate (0.04-0.4 degree/h) or rapid (>0.4 degree/h) (Sheikh et al., 2021). Alternatively, slope deformation analysis (e.g. FEM) can be used to estimate the magnitude of threshold movement (mm or degree) as warning criteria. In the developed platform in this study, users have the flexibility to configure either a critical threshold for slope movement (in degrees or millimeters) or a slope movement rate (in degrees per hour or millimeters per hour), as per their specific needs.

2.1.5 Weighted Hazard Index

In order to provide early warning based on an overall hazard index, that take into account all measurement results from different types of sensors (i.e. rainfall, pore-water pressure, soil moisture and deformation), a simplified weighting approach is proposed in this study. A normalization method was used to calculate the hazard warning index, W_i, for each sensor i as follows,

$$W_i = 100 \times \frac{(Y_i - T_{min,i})}{(T_{max,i} - T_{min,i})} \quad (4)$$

where W_i is the %warning, $T_{min,i}$ is the minimum reading of sensor i $T_{max,i}$ is the maximum reading of sensor i and Y_i is the current sensor reading at any given time (see Figure 4). By normalizing the sensor reading, the W_i varies between 0 and 100% corresponding to the prescribed minimum and maximum value of each sensor. The W_i value close to 100% indicates that the sensor reading is reaching the maximum value which corresponds to the critical value (e.g. the pore-water pressure at which factor of safety equal to 1 or critical rainfall intensity) set earlier in the platform. It should be noted that for tiltmeter or soil movement, both positive and negative sign can be equally critical. Hence the absolute value is used when calculating the warning index for soil movement as follows.

$$W_i = 100 \times \left| \frac{(Y_i - T_{min,i})}{(T_{max,i} - T_{min,i})} \right| \quad (5)$$

The overall warning index, OW, is then subsequently calculated by combining all the %warning, W_i, for each sensor from i to n, based on the significance weight x_i for each sensor as in the following.

$$\mathrm{OW} = \frac{\sum_{i=1}^{n} W_i \times x_i}{\sum_{i=1}^{n} x_i} \quad (6)$$

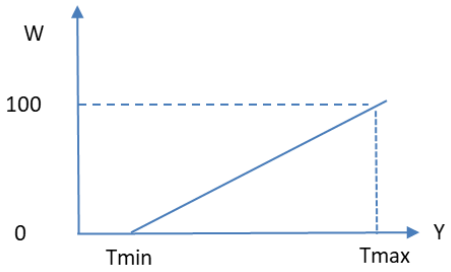

Figure 4 Normalization approach for sensor reading (Y) to the warning index W

The significance weight for each sensor, x_i, could be determined based on the level of confidence that each sensor holds, its accuracy, relative position on slope, the proximity of the sensor to critical zone, etc. The significance weight (x_i) assigned to each sensor is dynamic and can be fine-tuned within the platform. This flexibility enables adjustments to be made as needed. For instance, if a sensor were to experience a malfunction subsequently, its significance weight could be promptly adjusted to zero. This adjustment would result in the sensor's readings being excluded from the warning calculation. Any dynamic adjustment of the weight factors within the platform has to be done manually by experts. An illustrative example of this approach is provided in the following section.

3. KRATU-PATONG ROAD 2022 LANDSLIDE

3.1 Background

The Kratu-Patong Road landslide occurred on October 16, 2022, triggered by prolonged and heavy rainfall. The rainfall data from the closest weather station revealed a daily rainfall exceeding 150 mm, with a 3-day cumulative total surpassing 200 mm, as illustrated in Figure 3. This intense precipitation led to a slope failure, resulting in the complete collapse of one of the road lanes, as depicted in Figure 5.

Although the remaining road lanes were deemed precarious for commuters, substantial pressure emerged from both local authorities and private entities to reopen these lanes to the public. This urgency arose due to the fact that this road represented the sole accessible route to Patong Beach—an immensely popular beach resort town that attracts a high volume of tourists.

Figure 5 Road damage due to Kratu-Patong 2022 landslide in Phuket

Recognizing the immediate requirement, the Internet of Things (IoT) slope monitoring system, previously pioneered by the Geotechnical Innovation Laboratory at Kasetsart University, was swiftly deployed on-site as an interim solution. Its purpose was to furnish a reliable gauge for both local authorities and the Department of Highways. This data-driven insight would aid in making informed judgments regarding traffic management along the road during the ongoing slope stabilization endeavors.

3.2 Field Investigation and Sensor Installation

A rapid site investigation revealed that the depth to bedrock extended to approximately 6 meters, with the groundwater table positioned at a depth of 1.5 meters (as illustrated in Figure 6). The upper layer of soil was derived from biotite-muscovite granite and classified as brownish-to-whitish grey clayey sand. Previous study (Jotisankasa & Vathananukij, 2008) showed this granitic residual soil was prone to landslide and typically contained 3% gravel, 39% sand, 21% silt, and 37% clay. Our subsequent actions included the deployment of a piezometer at the 6-meter depth, a tensiometer at 2.67 meters, and two soil moisture sensors at depths of 0.1 meters and 0.5 meters. Additionally, three tiltmeters were strategically positioned on the back slope and along the water channel further upslope, along with the installation of a tipping bucket raingauge. It's worth noting that although the most suitable location for sensor installation would have been on the lower side of the slope, closer to the failed soil mass, operational constraints compelled us to install the sensor arrays on the upper side of the road, as visualized in Figure 7.

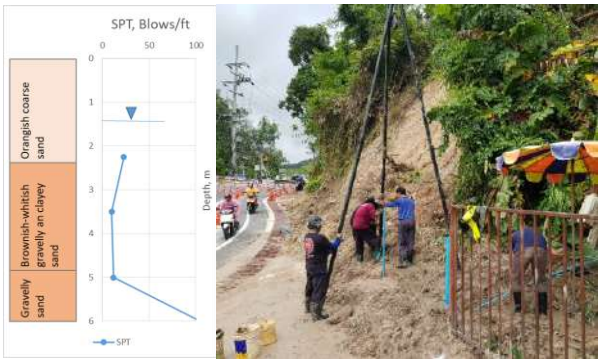

Figure 6 Soil investigation

Figure 7 Location of installed sensors; 1: Piezometer (6 m), 2: Tensiometer (2.67 m), 3: Tiltmeter (back slope), 4: Tiltmeter (upper channel), 5: Tiltmeter (water channel), 6: Soil moisture (0.1 m), 7: Soil moisture (0.5 m) and 8: Rain gauge

3.3 Stability Analysis and Warning Criteria

An unmanned aerial vehicle (UAV) survey was conducted with the objective of creating a three-dimensional model of the slope, employing the photogrammetry method. The resulting 3D model, as depicted in Figure 8, highlights the critical cross section that was then utilized for subsequent slope stability analysis. A uniform soil profile was specified based on in-situ SPT tests, with the strength parameters set as follows, effective cohesion, $c' = 10\ kPa$, angle of shearing resistance, $\phi' = 28^o$ and unit weight, $\gamma = 18\ \frac{kN}{m^3}$. Figure 9 presents the findings of the slope stability analysis, incorporating data from the monitored pore-water pressure profile alongside the assumed pore-water pressure values.

Figure 8 3D-model of the slope based on UAV survey

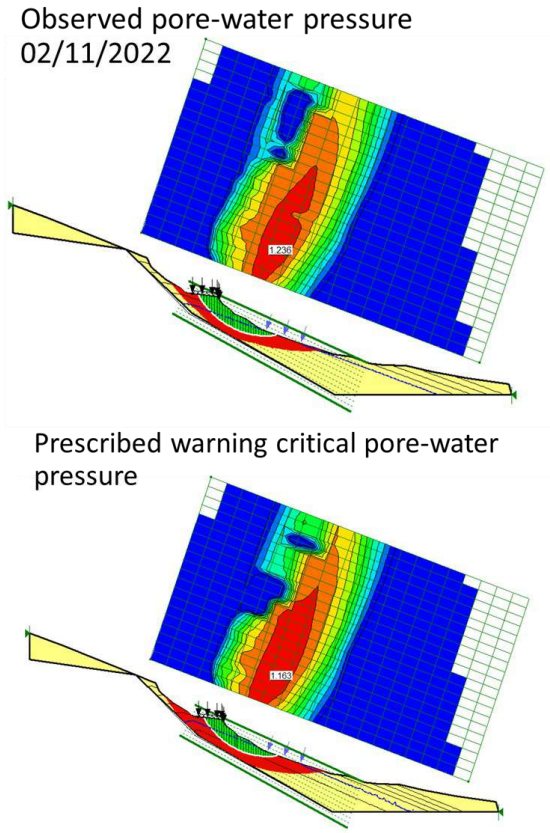

Figure 9 Stability analysis results

Significantly, we utilized monitored pore-water pressures, gathered from both piezometers and tensiometers, along with the spring line's emergence point on the lower slope to establish the pore-water pressure profile and phreatic line, as illustrated in Figure 10. Subsequent to this data compilation, a sequence of analyses was performed to derive the factor of safety variations in relation to pore-water pressure at the monitoring station's location. These findings are graphically depicted in Figure 11.

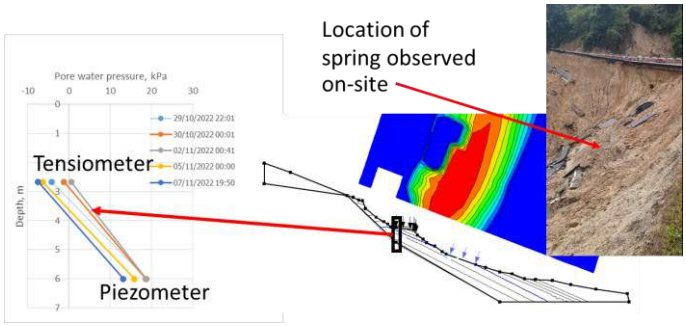

Figure 10 Pore-water pressure profile from monitoring results

Evidently, there exists a nearly linear relationship between the increase in pore-water pressure and the subsequent decrease in the factor of safety. To ensure a comprehensive analysis that considers the influence of road traffic, surcharge pressures of 10 or 20 kN/m^2 were incorporated. As an initial safety measure, we designated a pivotal indicator for slope instability warning: a threshold pore-water pressure of 30 kPa, specifically at a depth of 6 meters. This threshold is based on the slope stability analysis using the failed slope profile and a surcharge ranging between 10 and 20 kPa (Figure 11), corresponding to a factor of safety of approximately 1.15, providing a 15% margin of safety. Such threshold is related to such factors as soil strength parameters, unit weight, slope geometry and surcharge. It's worth noting that additional factors such as soil cover and rainfall contribute to the spatial and temporal variation of pore-water pressure within the slope, consequently influencing slope stability. While a detailed coupled rainfall stability analysis could shed light on this aspect, such an investigation lies beyond the scope of this study. The plant roots would also affect the shear strength and subsequently the threshold pore-water pressure. However, at 6 m depth the presence of plant roots is expected to be minimal and therefore the root cohesion is not considered in the calculation.

Furthermore, it's important to highlight that any increase in surcharge load significantly reduces the critical pore-water pressure threshold. This underscores the critical importance of restricting heavy traffic on the road while stabilization efforts were ongoing. To address this, a well-compacted earth berm was implemented by local authorities for stabilizing the collapsed slope. During construction, some traffic was permitted on the upper road due to pressure from the local community.

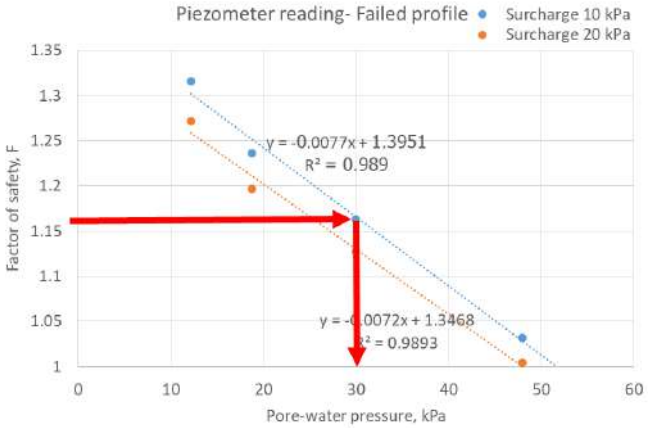

Figure 11 Variation between factor of safety and pore-water pressure from 6 m depth at the monitoring station

Notably, there was an approximately 45-day interim period between the slope collapse incident (16/10/2022) and the completion of stabilization berm (30/11/2022). During this time, continuous monitoring and daily reporting of the ongoing stability status were provided to the authorities to facilitate informed decisions regarding traffic management. It is worth mentioning that due to the ongoing alterations in the slope profile during the stabilization work, adjustments were made to increase the threshold of pore-water pressure. This adjustment was made to accommodate the additional safety margin offered by the presence of the berm using stability analysis of stabilized profile. Figure 12 depicts the variation in factor of safety with pore-water pressure between two slope geometries: the failed profile and the stabilized profile as of Date 19-11-22. By this date, approximately half of the buttress berm had been completed (as shown in Figures 12b and c), resulting in an increase in factor of safety and a partial relaxation of the threshold for critical pore-water pressure.

3.4 Warning Events

While the berm construction was in progress, there was mounting pressure to reopen the road lane for regular four-wheel vehicles.

Initially, only motorcycles were permitted on the road above the failed slope. On November 5, 2022, the road was gradually reopened for regular vehicles. However, this decision revealed signs of movement, as demonstrated by tiltmeter readings (Figure 13). These readings indicated initial backward movements (towards backslope) followed by downhill movement between November 10th and 11th, 2022.

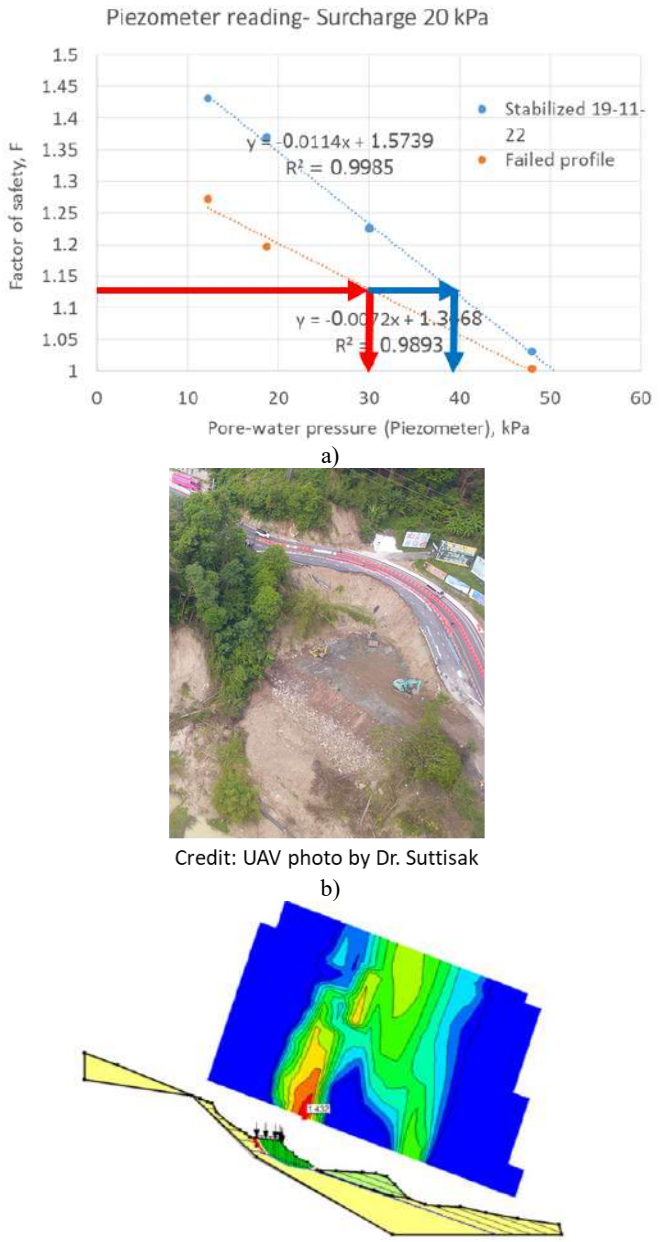

Figure 12 Increase in factor of safety due to stabilization work a) variation of factor of safety with pore-water pressure, b) UAV photos used to determine new slope geometry and c) slope profile as of Date 19-11-22 and stability analysis result

Notably, two out of three tiltmeters demonstrated a consistent response, suggesting the initiation of slope movement. The velocity of this movement was also computed on an hourly basis, expressed in degrees per hour, utilizing linear regression, as depicted in Figure 13b. Negative values signify movement towards the hill (backwards), whereas positive values denote downhill movement. Distinct spikes in movement were observed, with peak values ranging from -1.7 to 1.8 degrees per hour, notably triggered by increased traffic intensity. Such velocity exceeded the "rapid slope movement" threshold (>0.4 degree/hour) as suggested by Sheikh et al. (2021). This finding was further corroborated by an increase in pore-water pressure (or a decrease in suction) as recorded by the tensiometer (Figure 14). It is also interesting to note that the tensiometer could capture the increase in pore-water pressure in a negative range (in other words, the reduction in suction) due to the traffic-induced slope movement. In contrast, the piezometer failed to register any alteration in pore-water pressure unless the groundwater table ascended above the filter point. The consistent data from both types of sensors, namely, tensiometer and tiltmeter, served as a significant alarm, prompting us to initiate further discussions with local authorities. It should be noted that there was an increase in pore-water pressure due to rainfall earlier during 7 to 8/11/2022, though there was no sign of slope movement as no heavy traffic was still not allowed at the time.

While piezometers are valuable for monitoring pore-water pressure, relying solely on them has limitations. They may miss localized variations and rapid changes in pore-water pressure in the negative range especially at shallow depths, which can be crucial for detecting early signs of slope instability. Additionally, piezometers only capture one aspect of slope behavior, neglecting factors like excessive surcharge load, displacement, or runoff. To address this, our study proposes an IoT-based monitoring system integrating multiple sensors to provide a more comprehensive understanding of slope behavior, enabling better-informed decisions by geotechnical engineers.

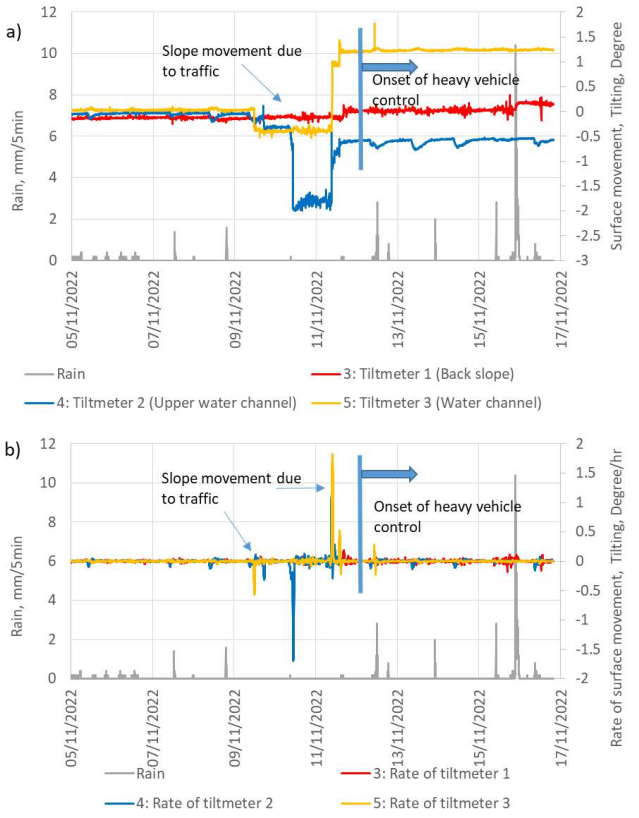

Figure 13 Tiltmeter readings and rainfall during the warning event

In light of these findings, the decision to reopen the road for four-wheel vehicles was swiftly reversed, and traffic control was reinstated, allowing only motorcycle users on the road. While this policy shift may have initially raised concerns among the public, it was grounded in engineering evidence, and the results from the instrumentation provided the public with greater confidence and understanding of the situation. Following the reinstatement of traffic control measures, the tiltmeter readings revealed no indications of further movement. This outcome bolstered our confidence in the decision that had been taken. The focus was then shifted to accelerating the berm construction to finish the stabilization work. Figure 15 provides a visual representation of the slope condition as it approached completion and afterward. It's important to note that the

slope monitoring instruments continued to operate, ensuring ongoing safety by detecting any movement on the backslope side.

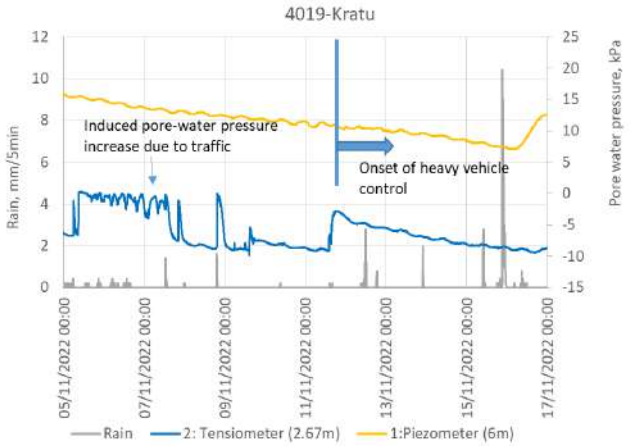

Figure 14 Pore-water pressure readings and rainfall during the warning event

The lessons learned from this incident have motivated our research team to develop a universal warning index derived from sensor data for automated hazard level indication. The weighted hazard index as explained earlier is one of such approaches. Figure 16 showed the calculated overall warning index, OW, based on parameters shown in Table 2. It is noted that the normalization and weight factors and threshold levels were re-adjusted in hindsight, after the warning event was over, to reflect the decision reached previously by expert panel during the incident. Regarding the soil movement measured using tiltmeters, there were two ways to calculate the warning index, namely Method 1 which used the absolute tilting (in degree) and Method 2 which utilized the absolute tilting rate (in degree per hour). The absolute values of tilting were used in calculating the warning index, W_i, for tiltmeter reading, since both toward-hill and down-hill directions could equally be a precursor to slope failure depending on the mechanism of the movement.

a)

b)

Figure 15 Slope condition in a) 28th November 2022; b) February 2023

Table 2 Normalization parameter and significance weight assumed for warning index calculation

Sensor, i	Unit	T_{min}	T_{max}	significance weight x_i
1:Piezometer (6 m)	kPa	0	30	2
2:Tensiometer (2.7 m)	kPa	-15	10	3
3: Tiltmeter 1 (Back slope)	Degree*	0	1	3
	Degree/hr **	0	0.4	3
4: Tiltmeter 2 (Upper water channel)	Degree*	0	1	3
	Degree/hr **	0	0.4	3
5: Tiltmeter 3 (Water channel)	Degree*	0	1	3
	Degree/hr **	0	0.4	3
6: Soil moisture (0.1 m)	%	0	42	1
7: Soil moisture (0.5 m)	%	0	42	1
Rain gauge	mm/5min	0	8	2

* Method 1; ** Method 2

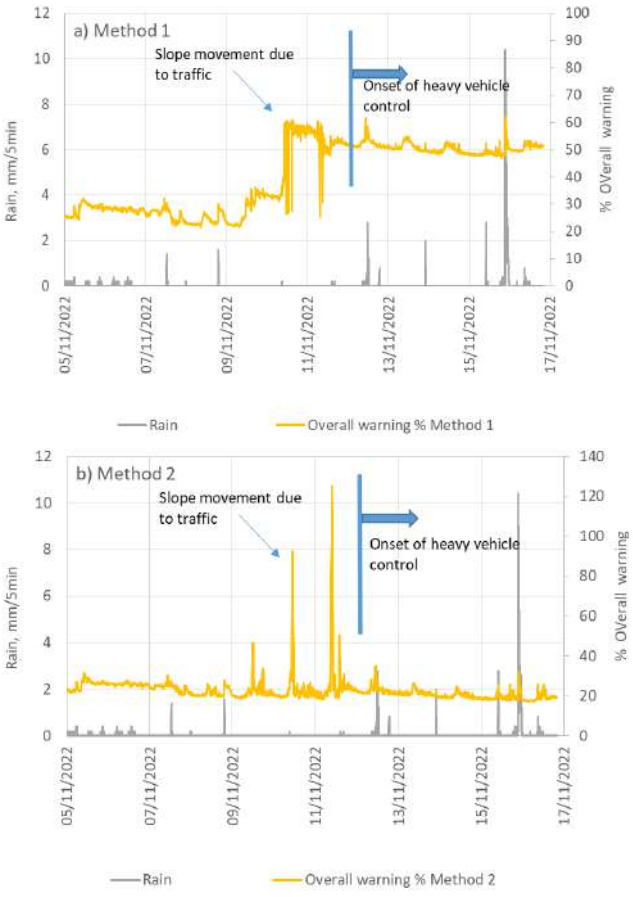

Figure 16 Overall warning index calculated using a) Method 1 and b) Method 2

Upon comparing the warning indices derived from Methods 1 and 2, it becomes evident that Method 1, relying on tilting magnitude, offers a continuous warning message. In contrast, Method 2, based on tilting velocity, issues a brief warning pulse lasting 1-2 hours, activated only when the velocity surpasses the predetermined threshold. The transient nature of Method 2's warning could

potentially be overlooked if not promptly addressed. Based on the warning event in this study using Method 1, the first alarm threshold for over warning could be set at 50% as indicated in Figure 16a.

In the context of Method 1, the warning message persists even after the slope has apparently returned to a safe condition, as observed from 12/12/22 onwards. This continuous alert will endure unless the tiltmeter's zero reading is manually reset, necessitating human intervention. It is clear that expert oversight in data presentation and reporting remains essential for ensuring the accurate representation of slope safety. The automated warning system is useful when no personnel could remain at their post all the times. To issue warning, panel discussion and expert judgement are still needed.

3.5 On-Going Monitoring Results

After the slope stabilization completion, the monitoring system has still been in operation until September 2023 and the results over the entire monitoring period are shown in Figures 17 to 20. During drying period spanning from January until May 2023, the pore-water pressure from the piezometer installed at 6 m depth (Figure 18) indicated only zero reading during the dry season due to the inherent limitation of the device as discussed earlier. A considerable rise in ground water table and positive pore water pressure could be observed on 19/08/2023 after the 1 day, 3 day and 7 day accumulated rainfalls reached the values of 14.8 mm, 42.6 mm and 262.6 mm respectively. However, the pore-water pressure at 2.67 m depth measured using the tensiometer (Figure 18) became more negative and reached the lowest value of about -50 kPa. The volumetric water content, as illustrated in Figure 19, peaked at approximately 42%, signifying saturation, and maintained a relatively stable level during the crucial period in December 2022. Following stabilization efforts, the soil surface was paved with concrete, expected to contribute to a reduction in infiltration. Subsequently, during the dry season, the water content decreased, reaching its lowest point at 30-35%. As the rainy season returned in 2023, the volumetric water content experienced a smaller peak at 39%, indicative of a less permeable surface.

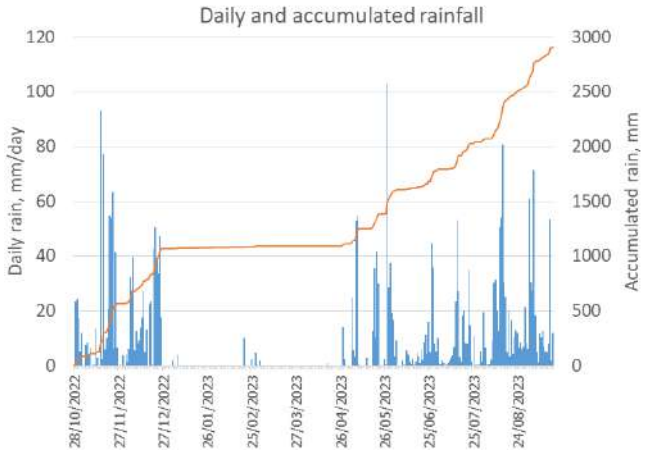

Figure 17 Daily rainfall and accumulated rainfall from Oct 2022 to Sep 2023

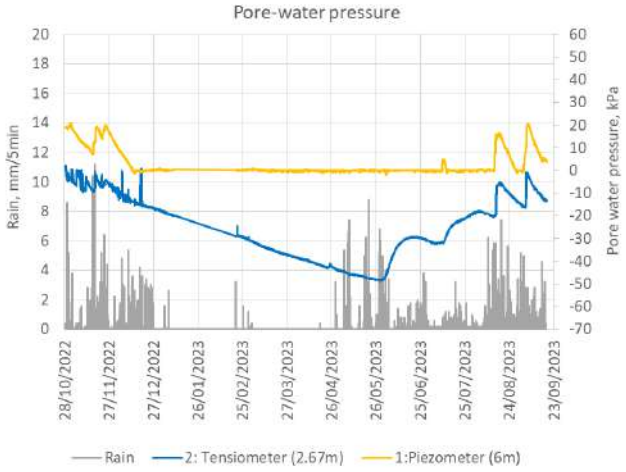

Figure 18 Pore-water pressure readings and 5 min rainfall from Oct 2022 to Sep 2023

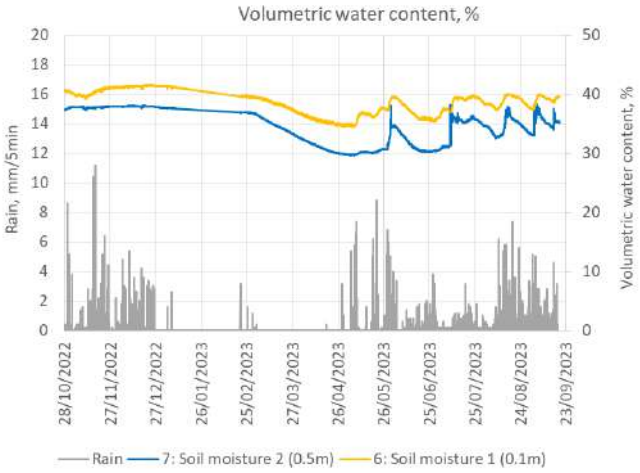

Figure 19 Volumetric water content and 5 min rainfall from Oct 2022 to Sep 2023

The slope movement throughout the entire monitoring period is illustrated in Figure 20, indicating a cessation of movement in the water channel at the crest of the stabilized slope (Sensor 5: Tiltmeter 3). This cessation persists despite heavy rainfall observed in the year 2023, underscoring the effectiveness of the stabilization efforts. However, noticeable movement is evident in the upper back slope, which remains unstabilized. By the end of September 2023, the tilting degree reached approximately 0.9 degrees. The average movement rate for the back slope was calculated at 0.126 degrees per month, equivalent to 0.000175 degrees per hour, categorizing it as a very slow movement according to Sheikh et al. (2021).

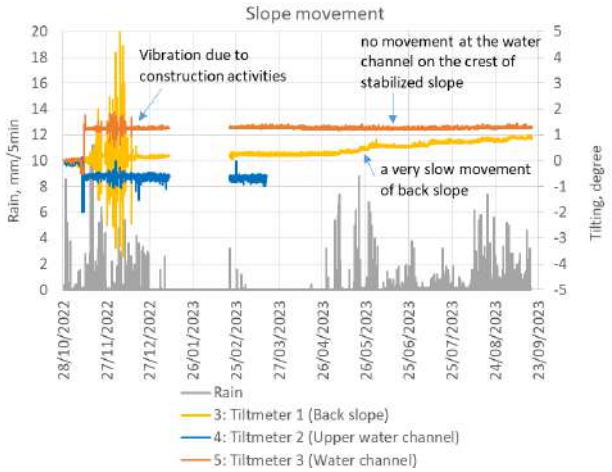

Figure 20 Slope movement and 5 min rainfall from Oct 2022 to Sep 2023

4. MODELLING OF SLOPE RESPONSE

In this section, a machine learning (ML) model, namely Artificial Neural Network (ANN), was used to predict the pore-water pressure at different depths based on various meteorological measurements, namely 5-min, 1-hour, 1-day, 3-day and 7-day antecedent rainfalls. The model was trained using the monitoring data from 4 November 2022 until 9 January 2023, 20% of which were used for testing, and the remaining 80% for training. The objective is to demonstrate correlation between rainfall parameters and pore-water pressure and to suggest ways to modelling them for cases in which any of the measuring equipment may not be available due to economical constraint. For instance, there are many slopes in Phuket where only rainfall data is available, yet none of the geotechnical measurement, such as pore-water pressure or slope movement, exists in those sites. Such ML models will be useful to provide a baseline prediction of pore-water pressure response for sites of similar condition. Only ML models were demonstrated in this section while the traditional seepage finite element modelling (e.g. Jotisankasa et al., 2015) was not included. This is because of the simplicity of the ML models and their readiness to be included with the existing IoT platform.

The neural network model architecture employed in this study was defined using the TensorFlow and Keras framework with Python code in Google Colab. The model was designed an input dimensionality of 5 and a 2-dimensional output as shown in Figure 21. The input nodes comprised of 5-min, 1-hour, 1-day, 3-day and 7-day antecedent rainfalls in mm, while the output nodes were pore-water pressure in kPa at depths of 6 and 2.67 m. The choice of specific antecedent rainfall intervals (5-min, 1-hour, 1-day, 3-day, 7-day) as input features for pore-water pressure prediction was based on the established research on critical rainfall envelopes (e.g., Lumb, 1975, Crozier & Eyles, 1980, Mairaing et al., 2012) as discussed in Section 2.1.3. The pore-water pressure is expected to be mainly influenced by both short-term and long-term antecedent rainfalls.

The neural network was constructed using the Sequential API, a straightforward way to build a linear stack of layers. This architecture is a type of feedforward neural network, where information flows unidirectionally from the input layer through the hidden layers to the output layer. The model comprises two dense (fully connected) layers. The first dense layer processed the input data using the rectified linear unit (ReLU) activation function. The first layer had 10 nodes, and each node was connected to the 5 input nodes. The second dense layer with a linear activation refined the representation obtained from the previous layer. This layer had 2 nodes, suitable for tasks requiring a 2-dimensional output. The model addresses the varying influences of rainfall on pore-water pressure at different depths by incorporating two separate output nodes for depths of 6 and 2.67 meters. This approach recognizes that the travel distance of the wetting front differs for each depth, impacting the response of pore-water pressure. To accommodate these differences, distinct weight factors and activation functions were utilized for each depth. The choice of ReLU activation in the first layer and a linear activation in the second layer aligned with common practices for regression tasks. The model was configured for training using the Adam optimizer with a custom learning rate of 0.01. The mean squared error loss function was employed for optimization.

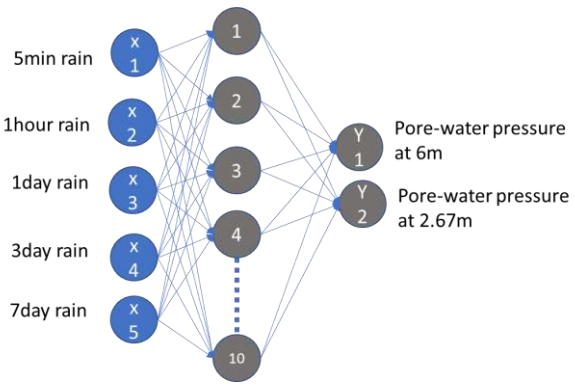

Figure 21 ANN model architecture used in this study

The predictive accuracy of the model is visualized in Figure 22. Key evaluation metrics, including the coefficient of determination (R^2) and root-mean-squared error (RMSE), were derived as 0.644 and 3.637 kPa, respectively. This level of fitting is deemed satisfactory for an initial phase, laying the foundation for future advancements in Artificial Neural Network (ANN) modeling within the Internet of Things (IoT) framework.

It is essential to note that the current ANN model's applicability and robustness is limited to sites with conditions resembling those present in the training dataset. Other site conditions of different geological settings and climates beyond the training dataset could affect the robustness of the model. As the dataset expands to encompass a more diverse range of slope types, geometries, and geological settings through extensive field monitoring, the ANN model can undergo refinement. This refinement process aims to enhance the model's reliability and accuracy, making it more robust for general application across varying conditions. This underlines the potential for ongoing developments in ANN modeling, fostering its integration into broader IoT platforms.

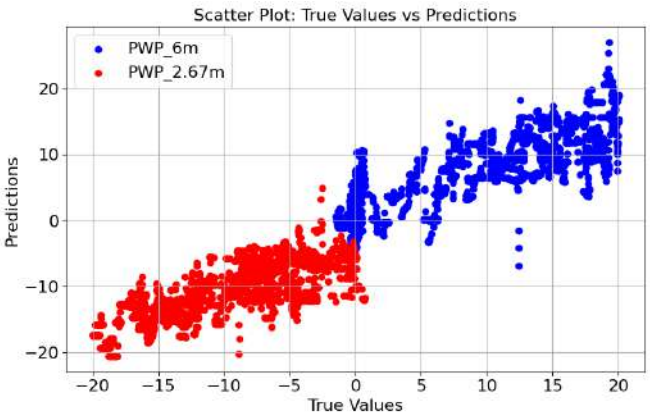

Figure 22 Comparison between the ML predictions and true values of pore-water pressure (in kPa) from two measurements at depths of 6 and 2.67 m

5. CONCLUSIONS

This paper explores the use of IoT sensor technology in geotechnical engineering, focusing on an ongoing IoT slope monitoring system in Thailand. The system employs various sensors like MEMs-based tensiometers, piezometers, and tiltmeters, all connected to an Arduino-based microcontroller using NB-IoT for data transmission to the cloud server. An application platform converts sensor readings into geotechnical parameters, aiding engineers in making informed decisions. The paper also introduces a weighted approach for calculating landslide hazard levels based on sensor data.

The Kratu-Patong Road landslide, triggered by heavy rainfall in October 2022, led to a road lane collapse and the implementation of an IoT slope monitoring system. Pressure to reopen the remaining lanes as the primary access route emerged, despite their riskiness. The warning event primarily arose from spikes in slope movement triggered by increased traffic intensity. Rapid slope movement during the incident involved a tilting magnitude of -2 to 1.2 degrees and a velocity ranging from -1.7 to 1.8 degrees per hour. Importantly, the continuous warning message derived from the calculation of the warning index based on tilting magnitude contrasts with an intermittent message based on tilting velocity. The tensiometer effectively identified the decrease in suction caused by slope movement, while the piezometer registered changes in pore-water pressure only when the groundwater table ascended above the measurement point. Ensuring the accurate portrayal of slope safety requires expert supervision in data presentation and reporting. The automated warning system proves valuable in situations where personnel cannot be present at all times. However, issuing warnings still necessitates panel discussions and expert judgment.

Additionally, an Artificial Neural Network (ANN) model was employed to predict pore-water pressure at various depths using 5

rainfall parameters (5-min, 1-hour, 1-day, 3-day, and 7-day antecedent rainfalls). The model exhibited satisfactory predictive accuracy (R^2 = 0.644, RMSE = 3.637 kPa), showing promising potential for future integration with the IoT platform.

6. ACKNOWLEDGMENTS

The authors express their gratitude for the funding support from Kasetsart University and the Department of Highways for the continuous development of the slope monitoring system. They also extend their appreciation to the dedicated teams from the Department of Highways, Kratu district, the municipality of Phuket province, and Green Ground Solutions, Co. Ltd, for their valuable assistance in the fieldwork. We would also like to acknowledge the use of ChatGPT, a language model developed by OpenAI, in refining the original draft of this paper. This paper is the expanded version of that presented at the Proc. of the 21st Southeast Asian Geotechnical Conference and 4th AGSSEA Conference (SEAGC-AGSSEA 2023).

7. REFERENCES

Buscarnera, G. & di Prisco, C. (2011). "Stability Criteria for Shallow Unsaturated Slopes." *Geotechnique Letters,* 1 (4), 85-90.

Cascini, L., Cuomo, S., Pastor, M & Sorbino, G. (2010). "Modelling of Rainfall-Induced Shallow Landslides of the Flow-Type." *Journal of Geotechnical and Geoenvironmental Engineering,* 136(1)

Crozier, M. J. and Eyles, R. J. (1980). "Assessing the Probability of Rapid Mass Movement." *Proc. 3rd Aus. NZ Conf. Geomech.*, *Wellington,* 2: 2.47–2.51.

Dunnicliff, J. and Green, G. E. (1988). "Geotechnical Instrumentation for Monitoring Field Performance." *Wiley.*

Jotisankasa, A., Mahannopkul, K., and Sawangsuriya, A. (2015). "Slope Stability and Pore-Water Pressure Regime in Response to Rainfall: a Case Study of Granitic Fill Slope in Northern Thailand." *Geotechnical Engineering Journal of the SEAGS & AGSSEA*, 46(1), 45-54.

Jotisankasa, A., Jamrueang, W., Pramusandi, S., Semmad, S., and Pilumwong, J. (2023). "Field Observations of Soil Moisture, Suction and Movement of Cornfield in Tropical Highland with and without Vetiver System." *8th International Conference on Unsaturated Soils (UNSAT 2023),* E3S Web of Conf., 382 (2023) 24004. DOI: https://doi.org/10.1051/e3sconf/202338224004.

Jotisankasa, A., Torsri, K., Supavetch, S., Sirirodwattanakool, K., Thonglert, N., Sawangwattanaphaibun, R., Faikrua, A., Peangta, P., Akaranee, J. (2023). "Investigating Correlations and the Validation of SMAP-Sentinel L2 and In Situ Soil Moisture in Thailand." *Sensors*, 23, 8828. https://doi.org/10.3390/s23218828.

Jotisankasa, A. and Vathananukij, H. (2008). "Investigation of Soil Moisture Characteristics of Landslide-Prone Slopes in Thailand." *Proc. of the International Conference on Management of Landslide Hazard in the Asia-Pacific Region, Sendai, Japan, November 11-15.*

Jotisankasa, A., Praphatsorn, W., Janthong, I., Sawangsuriya, A., and Jitareekul, P. (2023). "Development of IoT Slope Monitoring System and a Case History of Kratu-Patong Road Landslide in Phuket, Thailand." *Proc. of the 21st Southeast Asian Geotechnical Conference and 4th AGSSEA Conference (SEAGC-AGSSEA 2023)*, *25-26 October 2023, Bangkok, Thailand.*

Kankanamge, L., Jotisankasa, A., Hunsachainan, N., Kulathilaka, A. (2018). "Unsaturated Shear Strength of a Sri Lankan Residual Soil from a Landslide-Prone Slope and Its Relationship with Soil – Water Retention Curve." *International Journal of Geosynthetics and Ground Engineering*, 4 (3). DOI 10.1007/s40891-018-0137-7.

Lumb, P. (1975). "Slope Failures in Hong Kong." *Quarterly Journal of Engineering Geology*, 8: 31–65.

Mahannopkul, K. and Jotisankasa, A. (2019). "Influences of Root Concentration and Suction on Chrysopogon Zizanioides Reinforcement of Soil." *Soils and Foundations*, 59(2), 500 – 516. doi.org/10.1016/j.sandf.2018.12.014.

Mairaing, W., Jotisankasa, A. and Soralump, S. (2012). "Some Applications of Unsaturated Soil Mechanics in Thailand: An Appropriate Technology Approach." *Geotechnical Engineering Journal of the SEAGS & AGSSEA,* 43(1), 1-11.

Ridley, A. (2022). Delivering Data Diagnostics (making the most of geotechnical monitoring). *Thai Geotechnical Conference, Bangkok, Thailand.* 24-25 November 2022.

Sheikh MR., Nakata Y., Shitano M. and Kaneko M. (2021). "Rainfall-Induced Unstable Slope Monitoring and Early Warning through Tilt Sensors." *Soils and Foundations,* 61, 1033–1053.

Soralump, S., Shrestha, A., Thowiwat, W. Sukjaroen, R., Chaithong, T., Yangsanphu, S., Koirala, A., Jotisankasa, J. (2021). "Assessment of Landslide Behaviour in Colluvium Deposit at Doi Chang, Thailand." *Scientific Reports,* 11, 22960. https://doi.org/10.1038/s41598-021-02363-3.